Inorganic Chemistry

Article

pubs.acs.org/IC

Investigation of Fe incorporation in $LnCr_2Al_{20}$ (Ln = La, Gd, Yb) with ^{57}Fe Mössbauer and Single Crystal X-ray Diffraction

LaRico J. Treadwell,[†] Jacob D. McAlpin,[†] Devin C. Schmitt,[†] Michael J. Kangas,[†] Moulay T. Sougrati,[‡] Neel Haldolaarachchige,[§] David P. Young,[§] Jean-Claude Jumas,[‡] and Julia Y. Chan*,[†]

[†]Department of Chemistry, 232 Choppin Hall, Louisiana State University, Baton Rouge, Louisiana 70803, United States

[‡]Réseau sur le stockage électrochimique de l'énergie (RS2E) CNRS: FR3459, Centre National de la Recherche Scientifique, ICG Montpellier, AIME, France

[§]Department of Physics and Astronomy, 202 Nicholson Hall, Tower Drive, Louisiana State University, Baton Rouge, Louisiana 70803, United States

S *Supporting Information*

ABSTRACT: Crystal growth, structure determination, and magnetic properties of $LnCr_2Al_{20\text{-}x}Fe_x$ (Ln = La, Gd, Yb) adopting the $CeCr_2Al_{20}$ structure type with space group $Fd\bar{3}m$, $a \sim 14.5$ Å, are reported. Single crystal X-ray diffraction and Mössbauer spectroscopy are employed to fully characterize the crystal structure of $LnCr_2Al_{20\text{-}x}Fe_x$ (Ln = La, Gd, Yb). $LnCr_2Al_{20\text{-}x}Fe_x$ (Ln = La, Gd, Yb) are the first pseudoternaries adopting the $CeCr_2Al_{20}$ structure type with a transition metal occupying the main group site. The Yb analogues are Pauli paramagnets with the Yb ion adopting an electronic configuration close to Yb^{2+}, while the Gd analogues show paramagnetic behavior with no magnetic order down to 3 K.

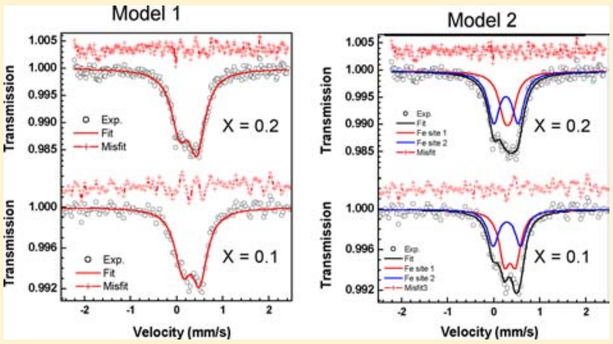

INTRODUCTION

The study of intermetallics containing rare earth, transition metal, and group 13 elements has attracted much attention due to the strong interaction of the conduction electrons with the local magnetic moments.[1] This can lead to interesting magnetic and electrical properties, including superconductivity, Kondo behavior, valence instability, heavy fermion behavior, and quantum criticality. Ytterbium-containing compounds are particularly intriguing due to the potential valence instability between the Yb^{3+} (f^{13}) and Yb^{2+} (f^{14}) states, and heavy fermion behavior has recently been observed in YbSi (ThAl structure type),[2,3] $YbCu_2Si_2$ ($ThCr_2Si_2$ structure type),[4,5] and YbT_2Zn_{20} (T = Fe, Co, Ru, Rh, Os, Ir; $CeCr_2Al_{20}$ structure type).[6,7] In addition, other members of the LnT_2Zn_{20} (Ln = lanthanides; T = Fe, Co, Ru, Rh, Os, Ir) series have been investigated, and it was found that the magnetic properties greatly depend on the transition metal present and the valence electron count.[7−10]

Isostructural LnT_2Al_{20} (Ln = lanthanides; T = Ti−Cr, Nb, Mo, Ta, W) compounds have also been reported.[11,12] Recently, it was found that $PrTi_2Al_{20}$ and PrV_2Al_{20} exhibits quadrupolar order at 2 and 0.6 K, respectively, while $PrCr_2Al_{20}$ shows Kondo behavior at low temperatures.[13−15] The SmT_2Al_{20} (T = Ti−Cr) analogues show valence fluctuations and order antiferromagnetically below 7 K.[16] GdV_2Al_{20} and $GdCr_2Al_{20}$ have also been shown to order antiferromagnetically at 2.35(5) and 3.90(5) K,[17] respectively, while CeT_2Al_{20} (T = Ti−Cr) and $YbCr_2Al_{20}$ are temperature independent paramagnets consistent with Ce^{4+} and Yb^{2+}, respectively.[18−20]

Due to the robust structure of the $CeCr_2Al_{20}$ structure type and the Frank−Kasper cages formed by the main group element, several different doping atoms have been incorporated onto different sites to investigate the effect on magnetic and electronic properties. $GdFe_2Zn_{20}$ has an abnormally high Curie temperature T_c at 86 K, while $GdCo_2Zn_{20}$ orders antiferromagnetically at 5.7 K. A doping study of Co for Fe, $Gd(Fe_xCo_{1\text{-}x})_2Zn_{20}$, was performed to study the ferromagnetic to antiferromagnetic ordering associated with the filling of the electronic states.[21] Also, Al was doped for Zn in $GdFe_2Zn_{20}$, which leads to a ferromagnetic ordering, but T_c decreases with increasing Al doping.[10] We focus our efforts on doping Fe into $LnCr_2Al_{20}$ (Ln = La, Gd, Yb) in order to investigate Fe site preferences. The parent analogues of La and Yb adopting the $CeCr_2Al_{20}$ structure type are diamagnetic and Pauli paramagnetic, respectively, while the Gd analogue shows antiferromagnetic ordering at 3.90(5) K.[17,22] Herein, we report the synthesis, crystal structure, Mössbauer results, and magnetic properties of the first pseudoternary of the $CeCr_2Al_{20}$-structure type where the transition metal dopant (Fe) substitutes for the main group element: $LnCr_2Al_{20\text{-}x}Fe_x$ (Ln = La, Gd, Yb).

Received: December 21, 2012
Published: April 19, 2013

EXPERIMENTAL SECTION

Synthesis. Single crystals of $LnCr_2Al_{20-x}Fe_x$ (Ln = La, Gd, Yb) were prepared using the molten metal flux technique using Ln (99.9%), Cr (99.996%), Fe (99.998%), and Al (99.999%) in various ratios. A ratio of 1:1.5:0.5:50 and 1:1:1:50 Ln:Cr:Fe:Al were used to prepare Yb and Gd analogues, respectively. The ratios of 1:1.5:0.5:100 and 1:1:1:100 for La:Cr:Fe:Al, respectively, were used to synthesize the La-analogue. For all reactions, the elements were placed in an alumina crucible, topped with a second alumina crucible, and then sealed inside an evacuated fused-silica tube. The samples were placed in an oven and heated to 1000 °C at 100 °C/h, dwelled for 24 h, and slowly (2 °C/h) cooled to 800 °C. The samples were then removed from the oven and centrifuged to remove excess flux. Residual flux was etched using (~1 M) NaOH. For the Yb-reactions, the lower Fe concentration (1:1.5:0.5:50) only yielded crystals adopting the $CeCr_2Al_{20}$ structure type (space group $Fd\bar{3}m$, $a \sim 14.5$ Å), with octahedral morphology up to 3 mm in length.[12] The larger Fe concentration (1:1:1:50) produced smaller crystals (≲1 mm^3) adopting the $CeCr_2Al_{20}$ structure type and bar-shaped crystals of the $YbFe_2Al_{10}$ structure type (space group $Cmcm$, $a \sim 8.966$ Å, $b \sim 10.153$ Å, $c \sim 9.003$ Å)[23] which could be separated based on morphology. As a result, higher concentrations of Fe were not attempted due to the presence of $YbFe_2Al_{10}$. The higher Fe-ratio of the Gd-synthesis yielded flat plates crystals (≲2.5 mm^3) adopting the $CeCr_2Al_{20}$ structure type, while the lower Fe-concentration yielded compounds adopting the $Ho_6Mo_4Al_{43}$ structure type (space group $P6_3/mcm$, $a \sim 10.975$ Å, $c \sim 17.611$ Å),[20] which was determined by single crystal X-ray diffraction. As a result, only one Fe doped Gd-compound is reported. Single crystals of the La-analogue were synthesized with an increased Al concentration to avoid the $Ho_6Mo_4Al_{43}$ structure type in order to stabilize the $CeCr_2Al_{20}$ structure type.

Structural Characterization. Single crystals of Fe-doped $LnCr_2Al_{20}$ (Ln = La, Gd, Yb) were cleaved and attached to a glass fiber. The fiber was then mounted on the goniometer of a Nonius Kappa CCD diffractometer with Mo Kα radiation ($\lambda = 0.710\,73$ Å). The diffraction pattern was indexed to a face-centered cubic unit cell with the lattice parameter $a \sim 14.5$ Å, consistent with the $CeCr_2Al_{20}$ structure type.[12] A multiscan absorption correction was applied to all data sets. The crystal structure was solved using SIR97[24] and refined with SHELXL97.[25] The final models were corrected for extinction, and atomic displacement parameters were modeled anisotropically. Collection and refinement parameters, atomic positions, and interatomic distances are provided in Tables 1−6, respectively. Refinement of the iron occupancies is discussed in the Results and Discussion section below.

Elemental Analysis. Elemental analysis was performed via energy dispersive X-ray spectroscopy (EDXS) using a JEOL JSM-5600 scanning electron microscope with an accelerating voltage of 15 kV. For all compounds, two polished crystals were measured four times each, and the results were averaged. The compositions, normalized to Ln, were $YbCr_{2.03(12)}Al_{25.01(18)}Fe_{0.10(3)}$, $YbCr_{1.77(23)}Al_{20.11(33)}Fe_{0.18(2)}$, $GdCr_{2.19(11)}Al_{24.23(17)}Fe_{0.28(6)}$, and $LaCr_{2.1(3)}Al_{25.1(6)}Fe_{0.2(1)}$. The crystals selected for EDS were also characterized by X-ray diffraction.

Magnetization and Electrical Transport. Single crystals selected for physical property measurements were first characterized by X-ray diffraction and EDS. Magnetic data were collected using a Quantum Design Physical Property Measurement System (PPMS). The temperature-dependent susceptibility data were measured under zero-field cooled (ZFC) conditions between 3 and 390 K with an applied field of 0.1 T. Field-dependent magnetization data were measured at 3 K with applied fields up to 9 T.

Mössbauer Spectroscopy. Single crystals used for physical property measurements were also used for Mössbauer spectroscopy. Powdered $YbCr_2Al_{20-x}Fe_x$ samples (x = 0.1 and 0.2) were analyzed at room temperature and at 77 K. The spectra were measured at two velocities (±2 and ±10 mm/s) with a constant-acceleration spectrometer which utilized a rhodium matrix cobalt-57 source and was calibrated at 300 K with α-iron powder. The Mössbauer spectral absorbers contained 20 mg/cm^2 of sample powder mixed with boron nitride. The quoted errors for the Mössbauer spectral parameters are the relative statistical errors.

Table 1. Crystallographic Parameters of $YbCr_2Al_{20\text{-}x}Fe_x$

formula	$YbCr_2Al_{20}$[a]	$YbCr_2Al_{19.9}Fe_{0.1}$	$YbCr_2Al_{19.8}Fe_{0.2}$
cryst syst	cubic	cubic	cubic
space group	$Fd\bar{3}m$	$Fd\bar{3}m$	$Fd\bar{3}m$
a (Å)	14.473(13)	14.450(4)	14.444(4)
V (Å^3)	3032(5)	3017.2(14)	3013.4(14)
Z	8	8	8
cryst dimensions (mm^3)	0.03 × 0.03 × 0.03	0.05 × 0.08 × 0.1	0.05 × 0.08 × 0.1
T (K)	293(2)	296(1)	296(1)
θ range (°)	2.44−29.85	3.99−29.91	3.99−29.92
μ (mm^{-1})	8.666	8.794	8.909
Data Collection			
measured reflns	701	1785	1552
unique reflns	248	247	247
reflns with $I > 2\sigma(I)$	224	223	230
R_{int}	0.0409	0.0384	0.0296
h	$-20 \leq h \leq 20$	$-20 \leq h \leq 20$	$-20 \leq h \leq 20$
k	$-14 \leq k \leq 14$	$-14 \leq k \leq 14$	$-14 \leq k \leq 14$
l	$-13 \leq l \leq 13$	$-13 \leq l \leq 13$	$-13 \leq l \leq 13$
Refinement			
$\Delta\rho_{max}$ (e Å^{-3})/ $\Delta\rho_{min}$ (e Å^{-3})	0.816/−1.24	0.862/−0.744	0.694/−0.769
GOF	1.167	1.062	1.185
extinction coeff	0.000 11(5)	0.000 35(5)	0.000 23(3)
reflns	248	247	247
params/restraints	17/0	21/3	21/3
R1 ($F^2 > 2sF^2$)[b]	0.0295	0.0215	0.0198
wR2 (F^2)[c]	0.0553	0.0456	0.0337

[a] Crystallographic data from ref 10. [b] $R1 = \Sigma||F_o| - |F_c||/\Sigma|F_o|$. [c] $R_w = [\Sigma[w(F_o^2 - F_c^2)^2]/\Sigma[w(F_o^2)^2]]^{1/2}$; $w = 1/[\sigma^2(F_o^2) + (0.0137P)^2 + 20.00P]$, $w = 1/[\sigma^2(F_o^2) + (0.0188P)^2 + 14.48P]$, $w = 1/[\sigma^2(F_o^2) + (0.0055P)^2\ ]$; $P = (F_o^2 + 2Fc^2)/3$ for $YbCr_2Al_{20}$, $YbCr_2Fe_{0.1}Al_{19.9}$, and $YbCr_2Fe_{0.2}Al_{19.8}$, respectively.

RESULTS AND DISCUSSION

Crystal Structure. The crystal structure of $GdCr_2Al_{20}$ is shown in Figure 1 and consists of a diamondlike network of Gd polyhedra and a pyrochlore-like network of Cr polyhedra. The $GdCr_2Al_{20}$ lattice parameter is 14.460(3) Å, and upon substitution of Fe for Al ($GdCr_2Fe_{0.3}Al_{19.7}$), the lattice parameter decreases to 14.4310(15) Å. The lattice parameter of $YbCr_2Al_{20}$ is 14.473(3) Å and decreases to 14.450(4) and 14.444(4) Å for $YbCr_2Fe_{0.1}Al_{19.9}$ and $YbCr_2Fe_{0.2}Al_{19.8}$, respectively, with the incorporation of the smaller iron atoms. The contraction of lattice parameters is a strong indication and consistent with Fe incorporated in the compounds.

The $GdCr_2Al_{20}$ crystal structure has one Gd site (8a), one Cr site (16d), and three Al sites (96g, 48f, 16c). The local environments of the five sites are depicted in Figure 2. The Gd polyhedron is 16 coordinate and is made up of 4 Al3 and 12 Al1 atoms with Gd−Al bond distances of 3.1307(6) and 3.2037(11) Å, respectively. The Gd polyhedron corner shares with 4 other Gd polyhedra with Gd−Gd distances of 6.269(6) Å. The Cr environment is 12-coordinate, forming a distorted icosahedron and is surrounded by 6 Al1 and 6 Al2 atoms with Cr−Al distances of 2.5631(5) and 2.7912(10) Å, respectively. Al1 (12-coordinate), Al2 (12-coordinate), and Al3 (14-coordinate) polyhedra, respectively, can be described as a

Table 2. Crystallographic Parameters of $LnCr_2Al_{20\text{-}x}Fe_x$ (Ln = La, Gd)

formula	$LaCr_2Al_{20}$	$GdCr_2Al_{20}$	$GdCr_2Al_{19.7}Fe_{0.3}$
cryst syst	cubic	cubic	cubic
space group	$Fd\bar{3}m$	$Fd\bar{3}m$	$Fd\bar{3}m$
a (Å)	14.552(1)	14.460(3)	14.431(1)
V (Å^3)	3081.5(6)	3023.5(11)	3005.3(5)
Z	8	8	8
cryst dimensions (mm^3)	0.02 × 0.08 × 0.1	0.05 × 0.08 × 0.1	0.03 × 0.08 × 0.1
T (K)	293(2)	293(2)	293(2)
θ range (°)	3.96−30.93	3.99−30.87	3.99−30.94
μ (mm^{-1})	5.229	6.89	7.8
Data Collection			
measured reflns	796	744	774
unique reflns	272	266	266
reflns with $I > 2\sigma(I)$	260	243	257
R_{int}	0.0133	0.0303	0.0135
h	$-21 \le h \le 21$	$-20 \le h \le 20$	$-20 \le h \le 20$
k	$-14 \le k \le 14$	$-14 \le k \le 14$	$-14 \le k \le 14$
l	$-13 \le l \le 13$	$-13 \le l \le 13$	$-13 \le l \le 13$
Refinement			
$\Delta\rho_{max}$ (e Å^{-3})/ $\Delta\rho_{min}$ (e Å^{-3})	0.827/−1.283	0.525/−0.761	0.634/−0.766
GOF	1.17	1.103	1.245
extinction coeff	0.000 32(5)	0.000 29(4)	0.000 36(5)
reflns	272	266	266
params/restraints	17/0	16/0	18/0
R1 ($F^2 > 2sF^2$)[a]	0.0247	0.0216	0.0161
wR2 (F^2)[b]	0.0649	0.0472	0.0418

[a] $R1 = \Sigma||F_o| - |F_c||/\Sigma|F_o|$. [b] $R_w = [\Sigma[w(F_o^2 - F_c^2)^2]/\Sigma[w\ (F_o^2)^2]]1/2$; $w = 1/[\sigma 2(F_o^2) + (0.0137P)^2 + 20.00P]$, $w = 1/[\sigma^2(F_o^2) + (0.0188P)^2 + 14.48P]$, $w = 1/[\sigma 2(F_o^2) + (0.0055P)^2]$; $P = (F_o^2 + 2F_c^2)/3$ for $LaCr_2Al_{20}$, $GdCr_2Al_{20}$, and $GdCr_2Fe_{0.3}Al_{19.7}$, respectively.

distorted bicapped pentagonal prism, a bicapped pentagonal prism, and a bicapped hexagonal prism, respectively. The Al−Al distances range from 2.6968(14) to 3.0935(8) Å, and are longer than the expected distance of 2.42 Å from covalent radii.[26]

Mössbauer Spectroscopy. Mössbauer spectra for $YbCr_2Al_{20\text{-}x}Fe_x$ (x = 0.1 and 0.2) are shown in Figure 3. An attempt to fit the data with only one iron site using one asymmetric doublet (model 1) leads to a difference in the experimental model and the calculated fit (misfit). The second attempt to fit the data with considering two iron sites (model 2) leads to a minuscule misfit compared to model 1, which suggests that our compound has two unique Fe-sites. In this case, the isomer shifts are quite similar while the quadrupole splittings corresponding to the two sites are clearly different, indicating that electronic charges are different for the two iron sites. Schematically, the quadrupole splitting is indicative of the site distortion; an iron atom occupying a regular geometry site will have a smaller quadrupole splitting and vice versa. Whichever the model used to fit the experimental data, the isomer shifts and the quadrupole splittings (provided in Table 7) are in the range of iron atoms in an intermetallic environment rich in aluminum[27−32] concluding that the Fe is substituting on Al sites.

Since model 2 has the best statistical data, we can conclude that there are two iron sites present. Model 2 suggests that the two iron sites can be distinguished on the basis of distortion in both compositions (x = 0.1 and 0.2). The site having the bigger quadrupole splitting (in blue shown in Figure 3) should correspond to the most distorted site. This model can only be explained if we assume that iron atoms go simultaneously into two aluminum crystallographic sites. Finally, Mössbauer spectra have been recorded at 77 and 300 K in a larger velocity range (Figure 4). The interest of recording spectra at such velocity (10 mm/s) is to check if there is any iron oxide. In fact, iron

Table 3. Atomic Positions of $YbCr_2Al_{20\text{-}x}Fe_x$

atom	site	symmetry	x	y	z	occ[b]	U_{eq} (Å^2)[c]
$YbCr_2Al_{20}$[a]							
Yb1	8a	$\bar{4}3m$	1/8	1/8	1/8	1	0.0139(3)
Cr1	16d	$\bar{3}m$	1/2	1/2	1/2	1	0.0078(4)
Al1	96g	mm	0.486 98(14)	1/8	1/8	1	0.0091(4)
Al2	48f	2mm	0.059 00(7)	0.059 00(7)	0.325 11(10)	1	0.0117(4)
Al3	16c	$\bar{3}m$	0	0	0	1	0.0182(8)
$YbCr_2Al_{19.9}Fe_{0.1}$[d]							
Yb1	8a	$\bar{4}3m$	1/8	1/8	1/8	1	0.0113(2)
Cr1	16d	$\bar{3}m$	1/2	1/2	1/2	1	0.0091(3)
Al1	96g	mm	0.058 99(5)	0.058 99(5)	0.325 25(8)	0.996(3)	0.0121(3)
Fe1	96g	mm	0.058 99(5)	0.058 99(5)	0.325 25(8)	0.004(3)	0.0121(3)
Al2	48f	2mm	0.4867(1)	1/8	1/8	0.992(5)	0.0099(4)
Fe2	48f	2mm	0.4867(1)	1/8	1/8	0.008(5)	0.0099(4)
Al3	16c	$\bar{3}m$	0	0	0	1	0.0204(7)
$YbCr_2Al_{19.8}Fe_{0.2}$[d]							
Yb1	8a	$\bar{4}3m$	1/8	1/8	1/8	1	0.010 02(16)
Cr1	16d	$\bar{3}m$	1/2	1/2	1/2	1	0.0081(2)
Al1	96g	mm	0.059 00(4)	0.059 00(4)	0.32519(6)	0.988(2)	0.0119(3)
Fe1	96g	mm	0.059 00(4)	0.059 00(4)	0.32519(6)	0.012(2)	0.0119(3)
Al2	48f	2mm	0.486 72(8)	1/8	1/8	0.988(4)	0.0093(4)
Fe2	48f	2mm	0.486 72(8)	1/8	1/8	0.012(4)	0.0093(4)
Al3	16c	$\bar{3}m$	0	0	0	1	0.0194(5)

[a] Crystallographic data from ref 10. [b] Site occupancy. [c] U_{eq} is defined as one-third of the trace of the orthogonalized U_{ij} tensor. [d] Composition obtained from refinement.

Table 4. Atomic Positions of $LnCr_2Al_{20-x}Fe_x$ (Ln = La, Gd)

atom	site	symmetry	x	y	z	occ[a]	U_{eq} (Å^2)[b]
$LaCr_2Al_{20}$							
La1	8*a*	$\bar{4}3m$	1/8	1/8	1/8	1	0.0123(2)
Cr1	16*d*	$\bar{3}m$	1/2	1/2	1/2	1	0.0096(3)
Al1	96*g*	*mm*	0.058 18(4)	0.058 18(4)	0.326 98(6)	1	0.0133(3)
Al2	48*f*	2*mm*	0.488 22(8)	1/8	1/8	1	0.0106(3)
Al3	16*c*	$\bar{3}m$	0	0	0	1	0.0272(6)
$GdCr_2Al_{20}$							
Gd1	8*a*	$\bar{4}3m$	1/8	1/8	1/8	1	0.0134(2)
Cr1	16*d*	$\bar{3}m$	1/2	1/2	1/2	1	0.0099(2)
Al1	96*g*	*mm*	0.058 75(4)	0.058 75(4)	0.325 77(6)	1	0.0122(2)
Al2	48*f*	2*mm*	0.487 03(8)	1/8	1/8	1	0.0106(3)
Al3	16*c*	$\bar{3}m$	0	0	0	1	0.0251(5)
$GdCr_2Al_{19.7}Fe_{0.3}$[c]							
Yb1	8*a*	$\bar{4}3m$	1/8	1/8	1/8	1	0.0133(1)
Cr1	16*d*	$\bar{3}m$	1/2	1/2	1/2	1	0.0113(2)
Al1	96*g*	*mm*	0.058 84(3)	0.058 84(3)	0.325 65(5)	0.97(2)	0.0147(3)
Fe1	96*g*	*mm*	0.058 84(3)	0.058 84(3)	0.325 65(5)	0.03(2)	0.0147(3)
Al2	48*f*	2*mm*	0.486 82(7)	1/8	1/8	1	0.0113(2)
Al3	16*c*	$\bar{3}m$	0	0	0	1	0.0278(5)

[a] Site occupancy. [b] U_{eq} is defined as one-third of the trace of the orthogonalized U_{ij} tensor. [c] Composition obtained from refinement.

Table 5. Select Interatomic Distances (Å) of $YbCr_2Al_{20-x}Fe_x$

compd	$YbCr_2Al_{20}$[a]	$YbCr_2Al_{19.9}Fe_{0.1}$	$YbCr_2Al_{19.8}Fe_{0.2}$
Yb 16 Coordinate			
Yb–Al3 (×4)	3.133(3)	3.1285(9)	3.1269(9)
Ln–Al1 (×12)	3.196(3)	3.1929(15)	3.1912(13)
Cr 12 Coordinate			
Cr–Al2 (×6)	2.565(2)	2.5615(7)	2.5605(7)
Cr–Al1 (×6)	2.804(3)	2.7977(14)	2.7965(12)
Al1 12 Coordinate			
Al1–Al2	2.702(2)	2.6945(19)	2.6941(16)
Al1–Al1	2.705(3)	2.699(2)	2.6972(19)
Al1–Al1 (×2)	2.745(3)	2.7434(19)	2.7418(16)
Al1–Cr	2.804(3)	2.7977(14)	2.7965(12)
Al1–Al2 (×2)	2.838(3)	2.8316(13)	2.8307(12)
Al1–Al1 (×2)	2.923(2)	2.9155(15)	2.9143(13)
Al1–Al3 (×2)	3.091(3)	3.0869(11)	3.0852(9)
Al1–Yb	3.196(3)	3.1930(13)	3.1913(11)
Al2 12 Coordinate			
Al2–Cr (×2)	2.565(2)	2.5615(7)	2.5602(7)
Al2–Al1 (×2)	2.705(3)	2.5615(7)	2.6941(16)
Al2–Al2 (×4)	2.825(3)	2.826(2)	2.824(2)
Al2–Al1 (×4)	2.838(3)	2.8316(13)	2.8306(12)
Al3 14 Coordinate			
Al3–Al1 (×12)	3.091(3)	3.0869(11)	3.0852(11)
Al3–Ln (×2)	3.133(3)	3.1287(9)	3.1269(9)

[a] Crystallographic data obtained from ref 10.

Table 6. Select Interatomic Distances (Å) of $LnCr_2Al_{20-x}Fe_x$ (Ln = La, Gd)

compd	$LaCr_2Al_{20}$	$GdCr_2Al_{20}$	$GdCr_2Al_{19.7}Fe_{0.3}$
Ln 16 Coordinate			
Ln–Al3 (×4)	3.1505(16)	3.1307(6)	3.1244(3)
Ln–Al1 (×12)	3.2446(10)	3.2037(11)	3.1949(8)
Cr 12 Coordinate			
Cr–Al2 (×6)	2.5780(13)	2.5631(5)	2.5581(3)
Cr–Al1 (×6)	2.7882(17)	2.7912(10)	2.7880(8)
Al1 12 Coordinate			
Al1–Al2	2.7197(19)	2.6968(14)	2.6894(12)
Al1–Al1	2.750(2)	2.7097(17)	2.7005(14)
Al1–Al1 (×2)	2.781(2)	2.7508(15)	2.7447(12)
Al1–Cr	2.7882(10)	2.7912(10)	2.7880(8)
Al1–Al2 (×2)	2.8373(10)	2.8292(10)	2.8248(7)
Al1–Al1 (×2)	2.9076(18)	2.9092(11)	2.9054(9)
Al1–Al3 (×2)	3.0896(8)	3.0935(8)	3.0859(5)
Al1–Yb	3.2017(1)	3.2037(1)	3.1949(7)
Al2 12 Coordinate			
Al2–Cr (×2)	2.5780(13)	2.5631(5)	2.5581(3)
Al2–Al1 (×2)	2.8373(10)	2.6968(14)	2.8248(7)
Al2–Al2 (×4)	2.8202(18)	2.8215(18)	2.8201(15)
Al2–Al1 (×4)	2.8373(10)	2.8292(10)	2.6894(12)
Al3 14 Coordinate			
Al3–Al1 (×12)	3.0915(7)	3.0935(8)	3.0859(5)
Al3–Ln (×2)	3.1508(4)	3.1307(4)	3.1244(3)

oxides give absorption peaks at around 8–9 mm/s which are not present in our spectra. From the results, we can also confirm the absence of any magnetic ordering between 77 and 300 K.

Crystal Structure Refinements. Because the Mössbauer results indicate two aluminum sites are occupied with iron, the X-ray diffraction models were re-examined to determine those sites. Bond lengths, atomic displacement parameters (ADP), and site occupancies can be useful in determining partial or mixed occupancy in extended solids. As shown in Table 5, all bond lengths decrease as a function of iron content, so the iron sites could not be identified in this manner. Similarly, no ADP values were found to be anomalous, and all refined sites were within ~1% of fully occupied. Therefore, to identify the Fe occupied sites, refinements were conducted with Fe occupying pairs of atomic positions. The total Fe in the unit cell was constrained to the EDS values, and the SUMP command in SHEXL was used to refine the iron occupancy of the two sites. Seven of the ten possibilities were successfully refined and gave similar quality metrics (*R* factors, goodness of fit, and residual electron density). The remaining three refinements were unstable or resulted in negative site occupancies. Sites were

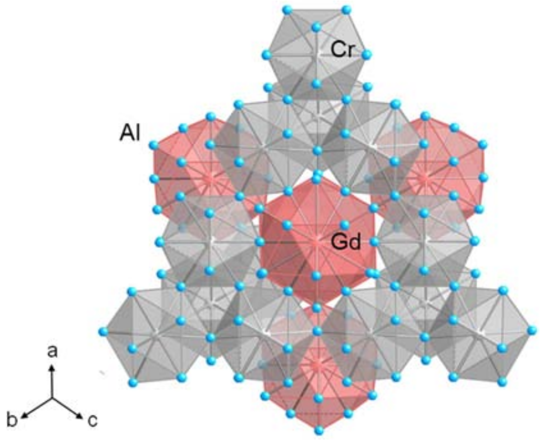

Figure 1. Crystal structure of $GdCr_2Al_{20}$ showing the interpenetrating network of the Gd and Cr polyhedra. The Gd polyhedra are shown as light pink, and the Cr polyhedra are shown as gray. Aluminum atoms are depicted as small light blue spheres.

designated as more ordered (higher symmetry) or disordered (lower symmetry) to compare to the Mössbauer results. The model with iron occupying the Al1 and Al2 sites gave the best agreement with the site occupancies of the more ordered and disordered sites obtained from Mössbauer spectroscopy. This analysis assumes that the Fe occupies the same two crystallographic sites in each of the two doping levels.

The Fe doped Gd-analogue has a site preference for iron that is different from the Yb-analogues. The Fe can only be refined for the Al1 site for the Gd-analogue. Modeling other Al sites with Fe leads to an unstable refinement model; thus, we cannot conclusively determine the presence of Fe on the Al2 site for the Gd-analogue. As far as the La-analogue, no Fe was modeled on any sites, indicating that Fe was not successfully substituted for Al or that the concentration of Fe is so minuscule that we are not able to distinguish it. Modeling Fe on any site in the La-analogue leads to an unstable refinement of the model.

Magnetization. Temperature dependent magnetic susceptibility data for $GdCr_2Al_{20\text{-}x}Fe_x$ are shown in Figure 5. The susceptibility for the three Yb compounds is nearly temperature independent consistent with nonmagnetic Yb^{2+}. This is similar to CeT_2Al_{20} (T = Ti−Cr) compounds,[18−20] which were also reported to be nearly temperature independent paramagnets. The doped and undoped Gd-analogues show no magnetic ordering down to 3 K, which is in contrast with previous literature that reported an antiferromagnetic ordering at 3.90(5) for $GdCr_2Al_{20}$.[17] A reason for the discrepancy is that previous magnetic data were measured on polycrystalline $GdCr_2Al_{20}$, and our present work is on single crystalline material, which allows us to directly measure intrinsic properties. Both the doped and undoped Gd-compounds yield μ_{eff} = 7.69(8) and 7.67(6) μ_B/Gd and Weiss constants of −8.22(6) and −5.31(2) K, respectively, by using the modified Curie−Weiss equation from 80 to 370 K. Although no magnetic ordering is apparent, the negative Weiss temperatures indicate a dominate antiferromagnetic exchange interaction between the Gd magnetic moments. The magnetic susceptibility of $LaCr_2Al_{20}$ is essentially temperature independent, which would indicate that Cr is nonmagnetic. There is no indication of magnetic ordering down to 3 K in any of the $LnCr_2Al_{20\text{-}x}Fe_x$ (Ln = La, Gd, Yb) analogues.

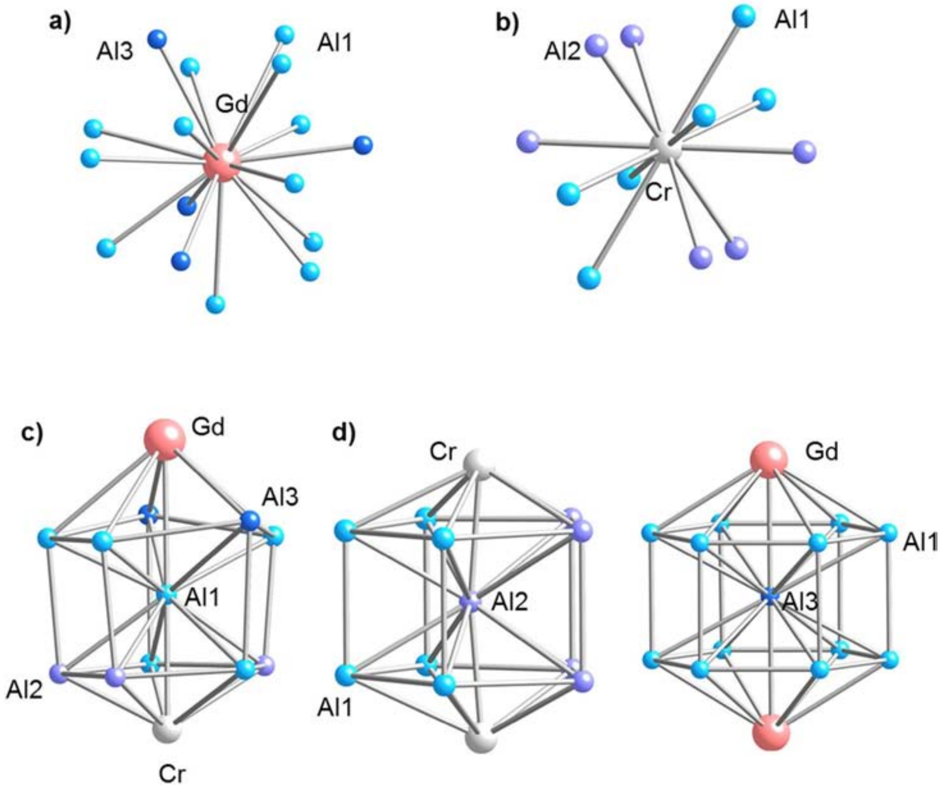

Figure 2. Local environments of Gd, Cr, Al1, Al2, and Al3 are shown in parts a−e, respectively. Gd atoms and Cr atoms are depicted as light pink spheres and gray spheres, respectively, while the Al1, Al2, and Al3 atoms are depicted as light blue, blue, and light purple, respectively.

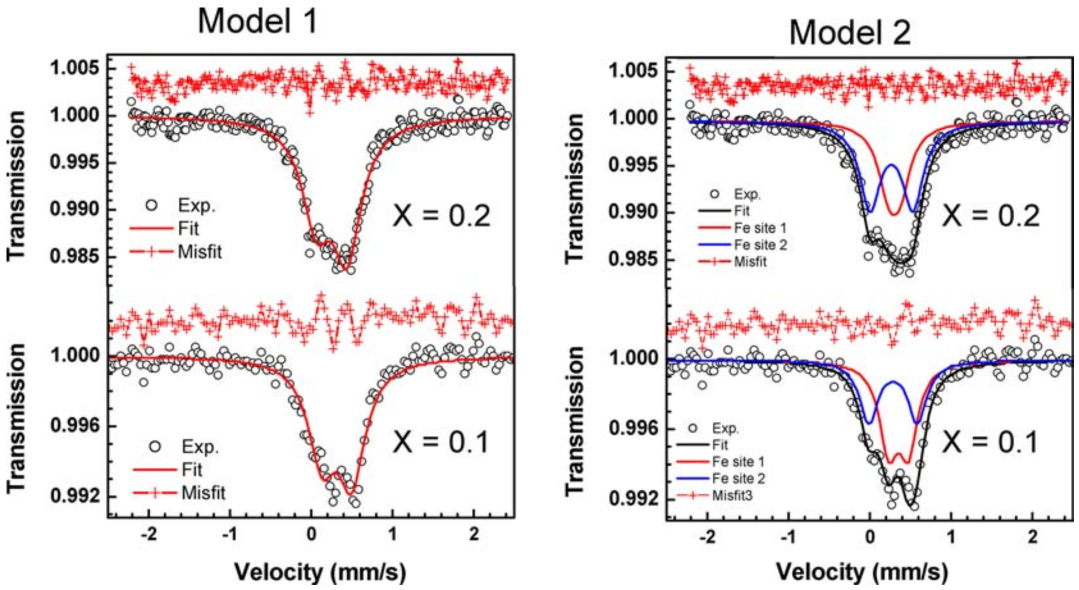

Figure 3. Room temperature Mössbauer data for $YbCr_2Al_{20-x}Fe_x$ samples (with x = 0.1 and 0.2) fitted with two different models as described in the text.

Table 7. Fitted Mössbauer Parameters for Spectra Measured at Room Temperature[a]

sample	IS (mm/s)	QS (mm/s)	LW (mm/s)	R.A. (%)
Fe = 0.2	0.31(1)	0.14(5)	0.31(3)	40(7)
	0.27(1)	0.53(3)		60(7)
Fe = 0.1	0.35(2)	0.24(3)	0.27(4)	57(6)
	0.28(2)	0.60(5)		43(6)

[a] IS, QS, LW, and R.A. are the isomer shift (relative to a-Fe at 300 K), the quadrupole splitting, the line width, and the relative areas, respectively.

Field dependent magnetization data (3 K) for $GdCr_2Al_{20-x}Fe_x$ are shown in Figure 6. The magnetization of $YbCr_2Al_{19.8}Fe_{0.2}$ and $YbCr_2Al_{19.9}Fe_{0.1}$ is very low and saturates at ~0.005−0.007 μ_B/mol at 9 T. The $GdCr_2Al_{20}$ and $GdCr_2Al_{19.7}Fe_{0.3}$ magnetization data show linear dependence as a function of field at low field (<3 T), which is typical of paramagnetic samples, and then begin to deviate around 6 μ_B/mol Gd, which is close to the saturation magnetization of Gd^{3+} (7 μ_B/mol) . The nearly identical form and magnitude of the field dependent magnetization data for both Gd analogues is a good indication that the Fe is nonmagnetic in the sample.

CONCLUSIONS

Single crystals of $LnCr_2Al_{20-x}Fe_x$ (Ln = La, Gd, Yb) were grown with molten aluminum flux. ^{57}Fe Mössbauer spectroscopy was essential in determining which sites the iron atoms occupied and indicated that the iron atoms occupied two distinct crystallographic sites. Crystallographic models were refined

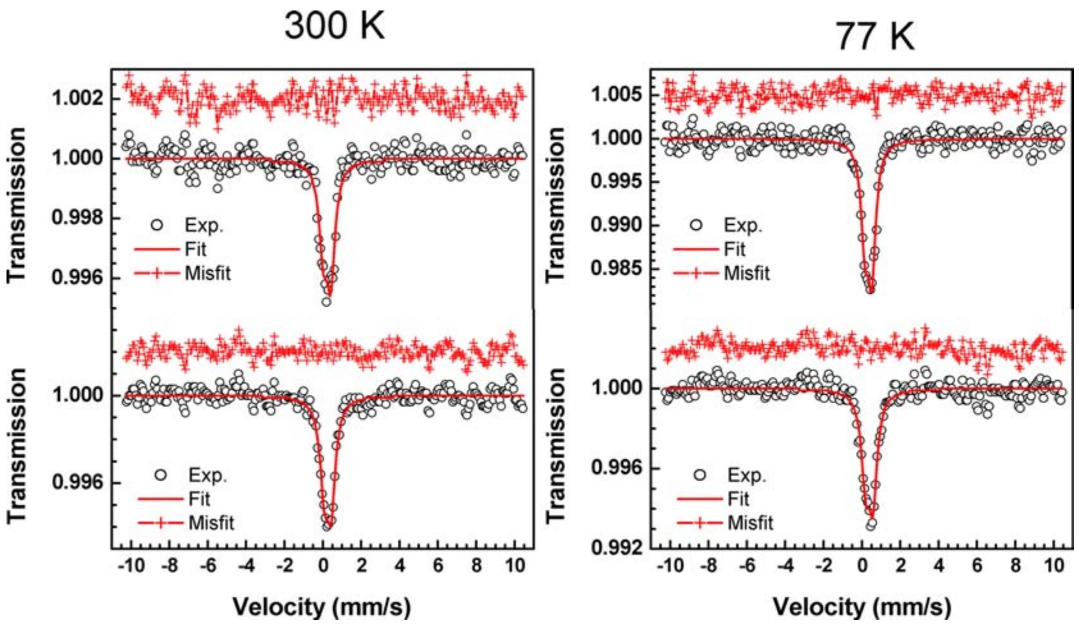

Figure 4. Mössbauer spectra at 300 and 77 K for $YbCr_2Al_{20-x}Fe_x$ samples (with x = 0.1 and 0.2).

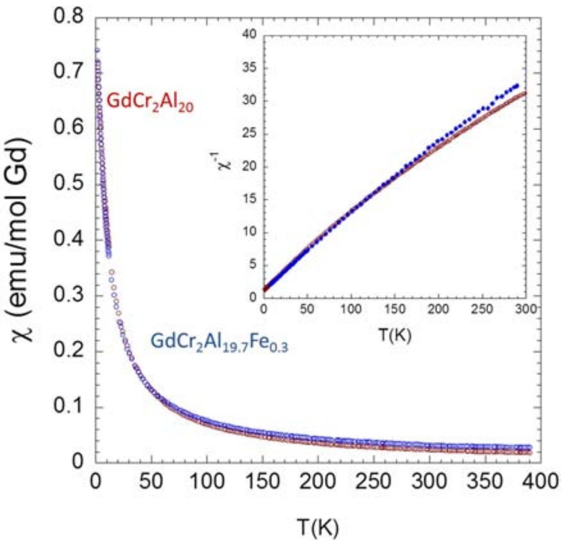

Figure 5. Temperature dependent magnetic susceptibility data for $GdCr_2Al_{20}$ and $GdCr_2Al_{19.7}Fe_{0.3}$.

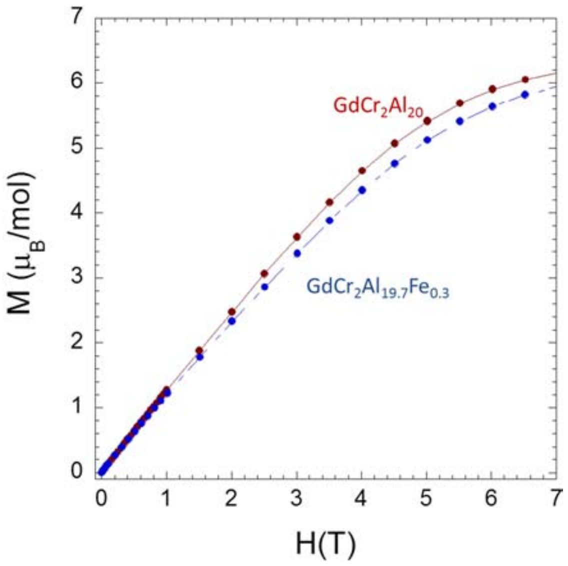

Figure 6. Field dependent magnetization data at 3 K are shown for $GdCr_2Al_{20}$ and $GdCr_2Al_{19.7}Fe_{0.3}$.

with Fe occupying each pair of crystallographic sites, and the best agreement with the Mössbauer spectroscopy was achieved when the Fe atoms partially occupied the Al1 (96*g*) and Al2 (48*f*) sites. The iron occupancy of the Al2 site remained fairly constant between the doping levels, while the iron occupancy of the Al1 site increased from ~0.5% to ~1.3% for the larger doping level. Single crystal X-ray diffraction data of the Fe doped Gd-analogues showed that Fe prefers to substitute for Al as opposed to a transition metal. Given the volume change with Fe substitution and the difference in atomic radii of the elements, it is reasonable to conclude that our model is suitable. On the basis of the atomic radii of Cr (1.249) and Fe (1.241), if Fe substitutes onto the transition metal site, we would expect a negligible change in volume. However, in our experiments, the volume of $GdCr_2Al_{20}$ (3023.5(11) Å^3) shows a decrease in volume upon substitution (3005.3(5) Å^3). This trend is also consistent with the Fe-doped Yb compounds as well. Due to the results of ^{57}Fe Mössbauer spectroscopy and single crystal X-ray diffraction data, we have successfully characterized the first pseudoternary intermetallic of the $CeCr_2Al_{20}$ structure type, where the Fe substitutes for the main group element. The results indicate that the latter transition metals (≥Fe) do not form LnT_2Al_{20} compounds adopting the $CeCr_2Al_{20}$ structure type, which can be rationalized by both atomic volume and valence electron count arguments.[20]

Like $YbCr_2Al_{20}$, both $YbCr_2Al_{20-x}Fe_x$ and $LaCr_2Al_{20}$ compounds display temperature independent magnetism. Due to the relative size of Gd, Fe can only be substituted on the Al1 site for $GdCr_2Al_{20-x}Fe_x$, unlike $YbCr_2Al_{20-x}Fe_x$ where the Fe substitutes on both the Al1 and Al2 sites. Single crystals of $GdCr_2Al_{20}$ and $GdCr_2Al_{19.7}Fe_{0.3}$ exhibit paramagnetic behavior down to 3 K with no magnetic ordering, while previously reported polycrystalline $GdCr_2Al_{20}$ displayed antiferromagnetic ordering at 3.90(5) K. This shows the importance of growing single crystals to determine the intrinsic magnetic properties of materials.

■ ASSOCIATED CONTENT

Ⓢ Supporting Information

Single crystal X-ray diffraction data in CIF format for $LnCr_2Al_{20-x}Fe_x$ (Ln = La, Gd, Yb). This material is available free of charge via the Internet at http://pubs.acs.org.

■ AUTHOR INFORMATION

Corresponding Author

*E-mail: jchan@lsu.edu.

Notes

The authors declare no competing financial interest.

■ ACKNOWLEDGMENTS

D.P.Y. acknowledges support from the National Science Foundation (NSF) through DMR1005764 and J.Y.C. acknowledges support from the NSF through DMR1063735.

■ REFERENCES

(1) Phelan, W. A.; Menard, M. C.; Kangas, M. J.; McCandless, G. T.; Drake, B. L.; Chan, J. Y. *Chem. Mater.* **2012**, *24*, 409−420.

(2) Engkagul, C.; Selim, R.; Mihalisin, T.; Schlottmann, P. *Phys. Rev. B* **1987**, *35*, 3686−3689.

(3) Bonville, P.; Gonzalez-Jimenez, F.; Imbert, P.; Jaccard, D.; Jehannot, G.; Sierro, J. *J. Phys.: Condens. Matter* **1989**, *1*, 8567.

(4) Tsujii, N.; Kitazawa, H.; Aoyagi, T.; Kimura, T.; Kido, G. *J. Magn. Magn. Mater.* **2007**, *310*, 349−351.

(5) Ōnuki, Y.; Yasui, S.; Matsushita, M.; Yoshiuchi, S.; Ohya, M.; Hirose, Y.; Dung, N. D.; Honda, F.; Takeuchi, T.; Settai, R.; Sugiyama, K.; Yamamoto, E.; Matsuda, T. D.; Haga, Y.; Tanaka, T.; Kubo, Y.; Harima, H. *J. Phys. Soc. Jpn.* **2011**, *80SA*, SA003.

(6) Torikachvili, M. S.; Jia, S.; Mun, E. D.; Hannahs, S. T.; Black, R. C.; Neils, W. K.; Martien, D.; Bud'ko, S. L.; Canfield, P. C. *Proc. Natl. Acad. Sci. U.S.A.* **2007**, *104*, 9960−9963.

(7) Canfield, P. C.; Jia, S.; Mun, E. D.; Bud'ko, S. L.; Samolyuk, G. D.; Torikachvili, M. S. *Physica B* **2008**, *403*, 844−846.

(8) Jia, S.; Ni, N.; Samolyuk, G. D.; Safa-Sefat, A.; Dennis, K.; Ko, H.; Miller, G. J.; Bud'ko, S. L.; Canfield, P. C. *Phys. Rev. B* **2008**, *77*, 104408.

(9) Tian, W.; Christianson, A. D.; Zarestky, J. L.; Jia, S.; Bud'ko, S. L.; Canfield, P. C.; Piccoli, P. M. B.; Schultz, A. J. *Phys. Rev. B* **2010**, *81*, 144409.

(10) Ni, N.; Jia, S.; Samolyuk, G. D.; Kracher, A.; Sefat, A. S.; Bud'ko, S. L.; Canfield, P. C. *Phys. Rev. B* **2011**, *83*, 054416.

(11) Niemann, S.; Jeitschko, W. *J. Solid State Chem.* **1995**, *114*, 337−341.

(12) Krypyakevich, P. I.; Zarechnyuk, O. S. *Dopov. Akad. Nauk. Ukr., Ser. A* **1968**, *30*, 364−366.

(13) Sato, T. J.; Ibuka, S.; Nambu, Y.; Yamazaki, T.; Hong, T.; Sakai, A.; Nakatsuji, S. *Phys. Rev. B* **2012**, *86*, 184419.

(14) Koseki, M.; Nakanishi, Y.; Deto, K.; Koseki, G.; Kashiwazaki, R.; Shichinomiya, F.; Nakamura, M.; Yoshizawa, M.; Sakai, A.; Nakatsuji, S. *J. Phys. Soc. Jpn.* **2011**, *80SA*, SA049.

(15) Ito, T. U.; Higemoto, W.; Nimomiya, K.; Luetkens, H.; Baines, C.; Sakai, A.; Nakatsuji, S. *J. Phys. Soc. Jpn.* **2011**, *80*, 113703.

(16) Sakai, A.; Nakatsuji, S. *Phys. Rev. B* **2011**, *84*, 201106(R).

(17) Verbovytsky, Y.; Latka, K.; Tomala, K. *J. Alloys Compd.* **2007**, *442*, 334−336.

(18) Kangas, M. J.; Schmitt, D. C.; Sakai, A.; Nakatsuji, S.; Chan, J. Y. *J. Solid State Chem.* **2012**, *196*, 274−281.

(19) Moze, O.; Tung, L. D.; Franse, J. J. M.; Buschow, K. H. J. *J. Alloys Compd.* **1998**, *268*, 39−41.

(20) Thiede, V. M. T.; Jeitschko, W.; Niemann, S.; Ebel, T. *J. Alloys Compd.* **1998**, *267*, 23−31.

(21) Jia, S.; Ni, N.; Samolyuk, G. D.; Safa-Sefat, A.; Dennis, K.; Ko, H.; Miller, G. J.; Bud'ko, S. L.; Canfield, P. C. *Phys. Rev. B* **2008**, *77*, 104408.

(22) Kangas, M. J.; Treadwell, L. J.; Haldolaarachchige, N.; McAlpin, J. D.; Young, D. P.; Chan, J. Y. *J. Solid State Chem.* **2013**, *197*, 523−531.

(23) Niemann, S.; Jeitschko, W. *Z. Kristallogr.* **1995**, *210*, 338−341.

(24) Altomare, A.; Burla, M. C.; Camalli, M.; Cascarano, G. L.; Giacovazzo, C.; Guagliardi, A.; Moliterni, A. G. G.; Polidori, G.; Spagna, R. *J. Appl. Crystallogr.* **1999**, *32*, 115−119.

(25) Sheldrick, G. *Acta Crystallogr.* **2008**, *64*, 112−122.

(26) Cordero, B.; Gomez, V.; Platero-Prats, A. E.; Reves, M.; Echeverria, J.; Cremades, E.; Barragan, F.; Alvarez, S. *Dalton Trans.* **2008**, 2832−2838.

(27) Fazakas, E.; Kane, S.; Lazar, K.; Varga, L. *Hyperfine Interact.* **2009**, *189*, 119−123.

(28) Preston, R. *Metall. Mater. Trans. B* **1972**, *3*, 1831−1835.

(29) Sério, S.; Waerenborgh, J. C.; Almeida, M.; Godinho, M. *J. Magn. Magn. Mater.* **2003**, *265*, 33−43.

(30) Shabashov, V. A.; Brodova, I. G.; Mukoseev, A. G.; Sagaradze, V. V.; Litvinov, A. V. *J. Phys.: Condens. Matter* **2007**, *19*, 386222.

(31) Waerenborgh, J. C.; Salamakha, P.; Sologub, O.; Sério, S.; Godinho, M.; Gonçalves, A. P.; Almeida, M. *J. Alloys Compd.* **2001**, *323−324*, 78−82.

(32) Zaleskia, A.; Fedotovaa, J.; Ilyuschenkob, A.; Talakob, T.; Belyaevb, A.; A., L.; Stanekc, J. *Acta Phys. Pol., A* **2006**, *109*, 441−444.